

# The quantum Hall effect and inter-edge state tunneling within a barrier

B.L. Johnson,<sup>1</sup> A.S. Sachrajda,<sup>2</sup> G. Kirczenow,<sup>1</sup> Y. Feng,<sup>2</sup> R.P. Taylor,<sup>2,3</sup> L. Henning,<sup>2</sup> J.  
Wang,<sup>2</sup> P. Zawadzki,<sup>2</sup> and P.T. Coleridge<sup>2</sup>

<sup>1</sup>*Department of Physics, Simon Fraser University, Burnaby, British Columbia, Canada V5A 1S6*

<sup>2</sup>*Institute for Microstructural Sciences, National Research Council, Ottawa, Ontario, Canada*

*K1A 0R6*

<sup>3</sup>*University of New South Wales, Kensington, NSW 2033, Australia*

## Abstract

We have introduced a controllable nano-scale incursion into a potential barrier imposed across a two-dimensional electron gas, and report on the phenomena that we observe as the incursion develops. In the quantum Hall regime, the conductance of this system displays quantized plateaus, broad minima and oscillations. We explain these features and their evolution with electrostatic potential geometry and magnetic field as a progression of current patterns formed by tunneling between edge and localized states within the barrier.

PACS numbers:73.40.Hm, 73.40.-c

Electronic transport in semiconductor systems of reduced dimensionality has been a field of great importance since the discovery of the quantum Hall effect by von Klitzing, Dorda, and Pepper.<sup>1</sup> They found that the Hall conductance of a two dimensional electron system at low temperatures is quantized, to remarkable precision, in integer multiples of  $e^2/h$ . Subsequently, Halperin,<sup>2</sup> Streda, et. al.,<sup>3</sup> Jain et. al.,<sup>4</sup> and Büttiker<sup>5</sup> proposed a theoretical picture in which the quantum Hall effect is seen as a manifestation of electrical conduction by magnetic edge states. These states appear at the boundaries of a macroscopic Hall bar in a strong magnetic field. Electrons that flow through them are immune to backscattering<sup>5</sup> in the quantum Hall regime, which results in the quantization of the Hall conductance and dissipationless transport. However, the edge states can be selectively backscattered if a potential barrier traverses the entire sample, as was demonstrated by Haug et al.,<sup>6,7</sup> who used this principle to elucidate the relationship between the quantum Hall effect and its breakdown, and the Landauer<sup>8</sup> theory of one-dimensional conduction. Experiments performed by Washburn et al.,<sup>9</sup> focused on the four-terminal conductance of a much smaller structure, a pair of narrow channels coupled by a barrier. These authors were also able to exploit backscattering from the barrier to study different transport quantization regimes, but they found that oscillatory conductance fluctuations, apparently arising from inhomogeneities in the electrostatic barrier potential, characterize the breakdown of quantization when it occurs.

The purpose of this paper is to report on an experimental study of the role of such a potential inhomogeneity, a depression introduced intentionally and in a controlled way in a potential barrier. We have been able to isolate the role of the internal structure of the depression in the transport problem experimentally, and propose a model that explains all of the phenomena that are observed as the potential depression gradually develops. We note that although the goal of this work is different, the structure that we have constructed represents a different method of measuring the transport properties of quantum dots, which have been discussed elsewhere.<sup>10</sup>

One of the most common techniques for fabricating low-dimensional devices is based on

the surface split gate technique developed by Thornton et al.<sup>11</sup> However, the geometries used have been constrained by the conventional methods used to contact surface gates. Recently, new techniques have been developed which for the first time enable isolated submicron gates to be contacted<sup>12,13</sup>, making the creation of a nanoscale depression possible. A schematic of our experimental gate geometry is shown in Fig. 1 a). The current path is from top to bottom in the figure. The gates 1, 2 and 3 are independently controlled. The depression is created by first applying a negative bias to gates 1 and 3 so as to just deplete the region of 2DEG between the gates. This creates a potential barrier. A *positive* voltage is then applied to gate 2, thus forming a depression (or ‘dimple’) in the barrier. A schematic cross-section of the barrier is shown in Fig. 1 b). The grid represents the electrostatic potential of the barrier, including the dimple. For magnetic fields which are not too small, certain edge states traverse the barrier, but manifest the shape of the underlying dimple potential. The heavy lines in Fig. 1 b) represent the edge states at the Fermi energy ( $E_F$ ). We note that the dimple is capable of supporting localised edge states, as depicted in the figure.

In Fig. 2 we show the experimental results for the conductance of the dimple structure as a function of applied magnetic field for constant side gate voltage and three different dimple gate voltages, at 50mK. The side gate voltage is held constant at  $-2.0V$ . The dimple gate voltages are  $+0.025V$  in *a*),  $+0.15V$  in *b*), and  $+0.4V$  in *c*), indicating the evolution of the conductance as the dimple becomes wider and deeper. Prominent features are the plateau at  $2e^2/h$ , labeled  $P_2$  in the figure, and the development, with increasing dimple potential, of a plateau approaching  $4e^2/h$ , labeled  $P_4$  (particularly for *b*) and *c*). Notice also the local minima, labeled  $M$  and  $W$ ;  $M$  for fields just below the onset of the  $P_2$  plateau in *a*) (nearly vanishing in *b*)), and  $W$  on the low-field side of the  $P_4$  plateau in *b*) and *c*). The inset to *b*) is an enlargement of the region around the point  $M$ . In *a*), the minimum is modulated by Aharonov-Bohm like oscillations, which persist onto the plateau  $P_2$ . As the dimple voltage is increased, the plateau  $P_2$  becomes more pronounced, the wide minimum  $M$  shrinks, and the transition from  $P_4$  to  $P_2$  becomes sharper (compare *a*) and *b*)). The developing wide minimum  $W$  for fields just below the  $P_4$  plateau in *b*) and *c*) also shows A-B oscillations,

as does the plateau itself. In general, as the dimple evolves, the conductance develops a progression of spin-unresolved plateaus ( $P_2$  and  $P_4$ ), preceded by A-B modulated, wide conductance minima ( $M$  and  $W$ , respectively). Finally, notice that the high-field end of the conductance plateau  $P_2$  drops off, also showing oscillations, and that the very low field conductance, while strongly modulated, increases with dimple voltage.

The nature of the transport problem in the dimple may be understood with the aid of a model based upon the schematic pictures of Fig. 3. Here the arrowed lines indicate the edge state configurations analogous to that in Fig. 1 b). The edge states are assumed to follow the electrostatic potential, and the dimple region supports localised edge states which are allowed due to the dimple potential below the center gate itself (compare Fig. 1). Higher (positive) dimple voltages widen and deepen the conducting region, allowing more edge states and/or localised states. The edge states and localised states are coupled together via unitary scattering events, represented by the dashed lines in Fig. 3. A feature of the present model is that the scattering probabilities are magnetic field-dependent in a manner that will be discussed below.

Our theoretical analysis of the above physical picture is a generalization of the edge-state scattering theories of Büttiker,<sup>14</sup> Kirczenow and Castaño,<sup>15</sup> and calculations in a geometry similar to that considered here, by Kirczenow;<sup>16</sup> a brief synopsis follows. The calculations are made at  $T = 0K$ . We assume that the current amplitude leaving any scattering event is related to the impinging current amplitude via a unitary scattering matrix. In addition, the current amplitude acquires a magnetic-field-dependent phase in transiting the path between scattering events. The current amplitude relationships, together with the unitarity constraint on the scattering matrices, generate a set of equations which may be solved for the current amplitudes leaving the sample in terms of the current amplitudes entering and the phase accumulated in circulating around the localised mode  $C$  in Fig. 3. The total transmission of the system (given by the square magnitude of the ratio of outgoing current amplitudes to incoming current amplitudes) may be calculated as a function of a dimensionless flux, which is the ratio of the flux threading the closed loop  $C$  (or  $C'$  as in Fig. 3

c)) to the flux quantum ( $h/e$ ) times  $2\pi$ , and is thus a function of both the area of the loop and the applied field. The conductance thus depends upon the width of the dimple (and thus the number of modes which traverse), as well as the magnetic field. Since exact knowledge of the potential geometry inside the barrier is impossible, the exact diameter of the localised edge state is unknown; however, estimates based upon the Aharonov-Bohm periods from Fig. 2 produce reasonable numbers for the sample geometry. For instance, an estimated dimple diameter of 500nm would give a conversion of roughly 1.3Telsa for every 10 in units of dimensionless flux. For clarity, the model calculations are left as a function of dimensionless flux, with this number as an approximate guide.

Results of the model calculation outlined above are given in Fig. 4. Here we plot the transmission as a function of dimensionless flux for three sets of parameters which correspond to the different configurations of edge states shown in Fig. 3. The theory plots in Fig. 4 a), b) and c) should be compared with the experimental data in Fig 2 a), b) and c), respectively, bearing in mind that the calculations are for  $T = 0K$ , and therefore the sharp narrow features will be smeared out by temperature. We begin with a qualitative discussion of the physics underlying the plot in Fig. 4 c), which will then be extended to the remaining plots shown in Fig. 4. In general, there are two main concepts in the model: *i*) the number of edge states decreases with increasing flux, which means that the higher Landau levels *depopulate* as the magnetic field pushes them through the Fermi energy; *ii*) at a given value of flux, the center gate voltage will control the depth and the width of the dimple. This will dictate how many localised states exist in the dimple, as well as how many edge states can traverse the dimple—generally, the wider (deeper) the dimple is, the more edge and localised states it can support.

In Fig. 4 c), we show the total transmission as a result of evolution from the configuration shown in Fig. 3 a) to Fig. 3 b) to 3 c) to 3 d) with increasing magnetic field. A generic, step-by-step picture of the model is as follows. At low fields (see Fig. 3 a)), there are three edge states impinging on the dimple from each direction, and a single localised state labeled  $C$ . The edge states  $B$  and  $D$  are coupled to the localised state via scattering at 1, 2, and 4.

As the field is increased, the state  $D$  depopulates, leaving the configuration shown in Fig. 3 b). At higher fields, the edge state  $B$  begins to pinch off and the state  $C$  depletes, since the magnetic field pushes the allowed levels up in energy, eventually pushing them through the Fermi energy, as mentioned above. This leads to the situation shown in Fig. 3 c), where the edge state  $B$  now couples to the new localised state  $C'$  (which has developed out of  $B$ ) only through 2 and 5, while edge state  $A$  couples to  $C'$  at the points of maximum curvature, as shown. From here, the edge state  $B$  depopulates, while at the same time the coupling between  $A$  and  $C'$  weakens and  $C'$  depopulates, leaving the situation depicted in Fig. 3 d). Here the edge states  $A$  and  $G$  are shown split into separate spin channels (the subscripts refer to “up” and “down”), since the field splits these in energy. The spin channel which is “against” the magnetic field will eventually depopulate. In the model we allow the down edge-states to couple via cross-channel scattering, which will be stronger for narrow structures (low dimple voltage).

In Fig. 4 c) we begin at low flux with the configuration of Fig. 3 a), with relatively strong coupling between states  $B, D, E, F$  and  $C$ , which is reasonable for high dimple voltage. The transmission is then calculated for the range of flux from 0 to 12 for this configuration and that in Fig. 3 b)—with increasing flux  $D$  and  $E$  depopulate, and thus coupling of  $D$  and  $E$  to  $C$  goes smoothly to zero (which results in the configuration of Fig. 3 b)). The wide conductance minima in the low-flux regime (an example is labeled  $W$  in Fig. 4 c), and in the experimental trace in Fig. 2 c)) are the result of interference between the closed loop states composed of state  $C$  and the possible loops including parts of  $C$  and parts of  $B$  and  $F$ . For example, in Fig. 3 b) the loop defined by the segments  $C1-C4-F4-F2-C1$  (here  $C1$  refers to the path  $C$  at the site labeled 1 in Fig. 3) has a different length than the path around loop  $C$ . The path length difference, and the corresponding difference in the phase accumulated in traversing the two paths, can lead to constructive or destructive interference between the two paths. The minimum  $W$  in Fig. 4 c) is the result of this interference.<sup>17</sup> For the range of flux 12 to 30, we begin with the configuration of Fig. 3 c), with strong coupling between all states, and let the scattering probabilities from the edge states to the localised

state go smoothly and monotonically to zero as inter-edge-state scattering is suppressed with increasing magnetic field. We let the scattering from  $B$  to  $C'$  at 2 and from  $F$  to  $C'$  at 5 vanish more quickly than the others, since the edge state  $B$  pinches off at lower fields than those which decouple state  $A$  from  $C'$ . The regular conductance oscillations at  $P_4$  (compare the inset of Fig. 2 c)) are due to Aharonov-Bohm like interference. The drop in conductance from near  $4e^2/h$  at  $P_4$  to  $2e^2/h$  at  $P_2$  is the result of the pinch-off of modes  $B, F$ , followed by the decoupling of  $A, G$  from mode  $C'$ . The persistence of the latter coupling can have interesting effects, as discussed below. Finally, the oscillatory structure at the high-flux end (c.f. Fig. 2 a)) is due to closed-loop interference as the spin-down channel pinches off, i.e. the scattering probability between the spin-down modes across the structure (the dashed lines in Fig. 3 d)) approaches 1.

The theoretical conductances depicted in Fig 4 a) and b) are calculated in the same manner as above (ie, the *basic steps are the same*), with some important differences caused by the lower dimple voltage. In Fig. 4 b), we assume that the coupling of  $D, E$  to  $C$  at 2, 5 is weaker than in Fig. 4 c), consistent with the lower dimple voltage (narrower structure), while in Fig 4 a) we assume that the initial configuration is given by Fig. 3 b); again the lower dimple voltage allows for fewer edge states initially. In Fig. 4 a), the lower overall conductance at  $P_4$  is due to weaker coupling between  $C'$  and  $B, F$  in Fig. 3 c), since here again the structure is narrower and the difference in energy between levels is greater. The minima marked  $M$  in Fig. 4 a) and b) have the same origin as the wide minimum marked  $W$  in c): after modes  $B, F$  in Fig. 3 c) depopulate, the configuration is exactly like that of Fig. 3 b), with one less edge state. The resulting oscillatory structure at  $M$  is due to the persistent coupling of  $A, G$  to  $C'$  as mentioned above. This is especially apparent in Figs. 4 a) and 2 a), but is also visible in 4 b) and 2 b).

In general, comparing the experimental and theoretical pictures reveals the following. A developing conductance plateau  $P$  is preceded on the low-field side by a local minimum  $M$  or  $W$ , which is modulated by Aharonov-Bohm like oscillations. These minima are the result of interference between edge states and localized states in the dimple—compare the features

marked  $M$  and  $W$  in Fig. 2 and Fig. 4. Also, more plateaus develop with higher dimple voltage as more edge states are allowed. The evolution of the small plateau near  $4e^2/h$  (labeled  $P_4$ ) in the experimental data is a result of the wider dimple created by higher gate voltage. In the model, this widening has two consequences: the initial coupling of  $B$  and  $F$  to  $C$  in the configuration of Fig 3 c) is stronger, and the couplings between modes decay more rapidly with increasing flux (a consequence of the dimensionless flux having the area of the dimple built-in. The field required to de-populate levels goes down as area increases). The overall effect is the appearance of a hump ( $P_4$ ), and then a short plateau—compare Fig 2 b) and c), comparing the labeled features. The short plateau  $P_4$  is still modulated by A-B oscillations, which are the result of the remaining coupling and interference. Note that  $P_4$  narrows with increasing dimple voltage in both experiment and theory.

In summary, we have presented an experimental study of the magneto-conductance of a dimple, a structure formed by gradually imposing a sub-micron scale depression in a potential barrier across a 2DEG. The role of the dimpled potential barrier in the backscattering of magnetic edge states and the quantum Hall effect is studied in a controlled fashion. We find that scattering and interference between edge states and localised states within the dimple produces a set of broad minima and oscillations in the conductance as a function of magnetic field.



## REFERENCES

- <sup>1</sup> K. von Klitzing, G. Dorda and M. Pepper, Phys. Rev. Lett. **45** 494 (1980)
- <sup>2</sup> B.I. Halperin, Phys. Rev. B **25**, 2185 (1982)
- <sup>3</sup> P. Streda, J. Kucera and A.H. MacDonald, Phys. Rev. Lett. **59**, 1973 (1987)
- <sup>4</sup> J.K. Jain and S.A. Kivelson, Phys. Rev. Lett. **60**, 1542 (1988)
- <sup>5</sup> M. Büttiker, Phys. Rev. B **38**, 9375 (1988)
- <sup>6</sup> R.J. Haug, A.H. MacDonald, P. Streda, and K. von Klitzing, Phys. Rev. Lett **61**, 2797 (1988)
- <sup>7</sup> R.J.Haug, J.Kucera, P. Streda, and K. von Klitzing, Phys. Rev. B **39**, 10892 (1989)
- <sup>8</sup> R. Landauer, IBM J. Res. Dev. **1**, 223 (1957)
- <sup>9</sup> S. Washburn, A.B. Fowler, H. Schmid, and D. Kern, Phys. Rev. Lett. **61**, 2801 (1988)
- <sup>10</sup> B.J. van Wees, et al., Phys. Rev. Lett. **62**, 2523 (1989)
- <sup>11</sup> T.J. Thornton, et al Phys. Rev. Lett. **56**, 1198 (1986)
- <sup>12</sup> P.J. Simpson, et. al, Appl. Phys. Lett. **63**, 3191 (1993); P.J. Simpson, et. al, unpublished;  
C.J.B. Ford, et. al, unpublished
- <sup>13</sup> Y. Feng et al, Appl. Phys. Lett. **12**, 1666 (1993)
- <sup>14</sup> M. Büttiker, Semiconductors and Semimetals **35**, 191 (1992)
- <sup>15</sup> G. Kirczenow and E. Castaño, Phys. Rev. B **43**, 7343 (1991)
- <sup>16</sup> G. Kirczenow, Phys. Rev. B , 1111 (1994)
- <sup>17</sup> Quantum interference due to successive scattering events between a pair of states traveling  
in the same direction was first observed by C.J.B.Ford, et. al, Phys. Rev. B **43**, 7339 (1991)

## FIGURES

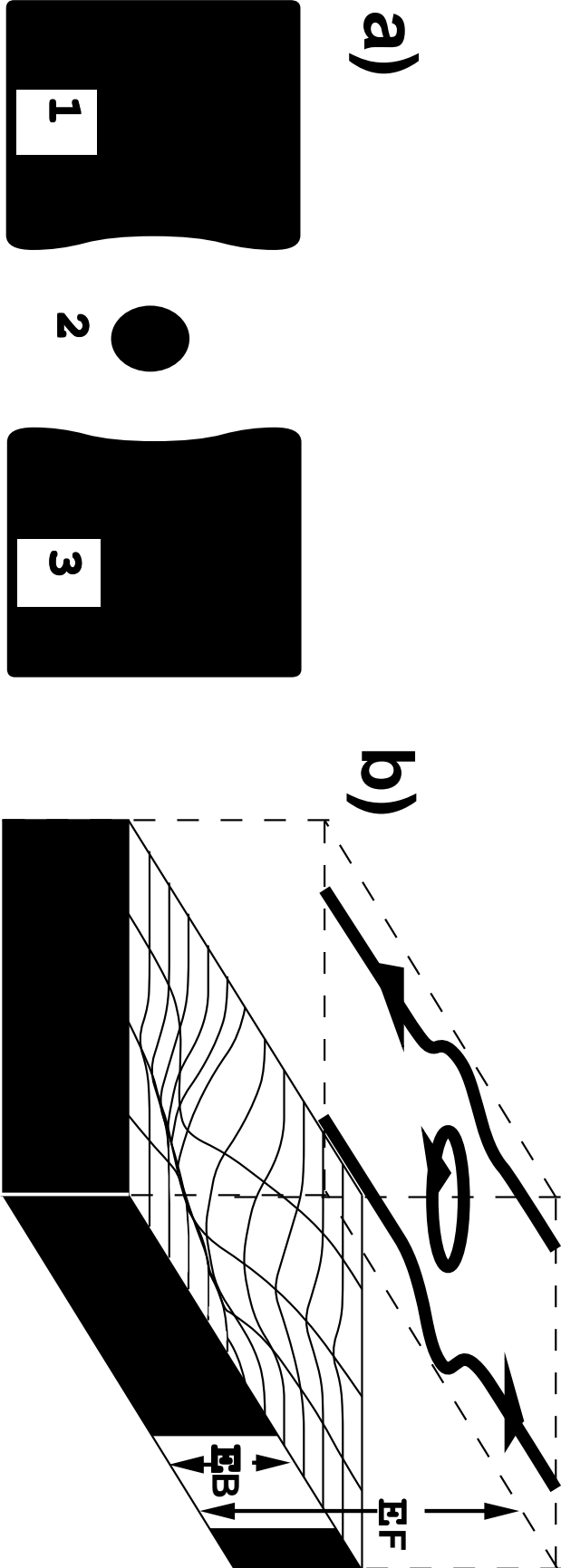
FIG. 1. a) Schematic of the experimental geometry. The dark areas represent the gates. All gates are individually controlled. For the experiments reported here, gates 1 and 3 are biased with negative voltage creating a potential barrier, then a positive bias is applied to the center gate 2, creating the dimple in the potential barrier. The gate 2 has a diameter of 300nm, and gates 1 and 3 are separated by 850 nm. The GaAs/AlGaAs wafer was delta doped with a Si donor density of  $1.5 \times 10^{12} \text{cm}^{-2}$  separated from the 2DEG by a  $400\text{\AA}$  spacer layer. The density and mobility after illumination were  $3.3 \times 10^{11} \text{cm}^{-2}$  and  $1.5 \times 10^6 \text{cm}^2/\text{Vs}$ , respectively. The gates are made from *Ti/Pt/Au* alloy. b) Schematic of the profile (grid) and the resulting edge states. For reference, the barrier height ( $E_B$ ) and the Fermi level ( $E_F$ ) are shown.

FIG. 2. Experimental results for the conductance as a function of magnetic field for three different center gate voltages. Here the side gates are maintained at  $-2V$ , while the center gate is varied: a)  $0.025V$ , b)  $0.15V$  and c)  $0.4V$ .

FIG. 3. Model configurations considered in this paper. Here the arrowed lines are edge states (compare Fig. 1 b)), and the dashed lines represent inter-state scattering. The labels are defined in the text. In c), the subscripts refer to spin.

FIG. 4. Results of the model calculations described in the text. Note the labeled features for comparison to the experimental data of Fig. 2. The dimensionless flux is given by the ratio of the magnetix flux through the closed loop paths of Fig. 3 to the flux quantum times  $2\pi$ , as discussed in the text.

**Figure 1**









**Figure 2**

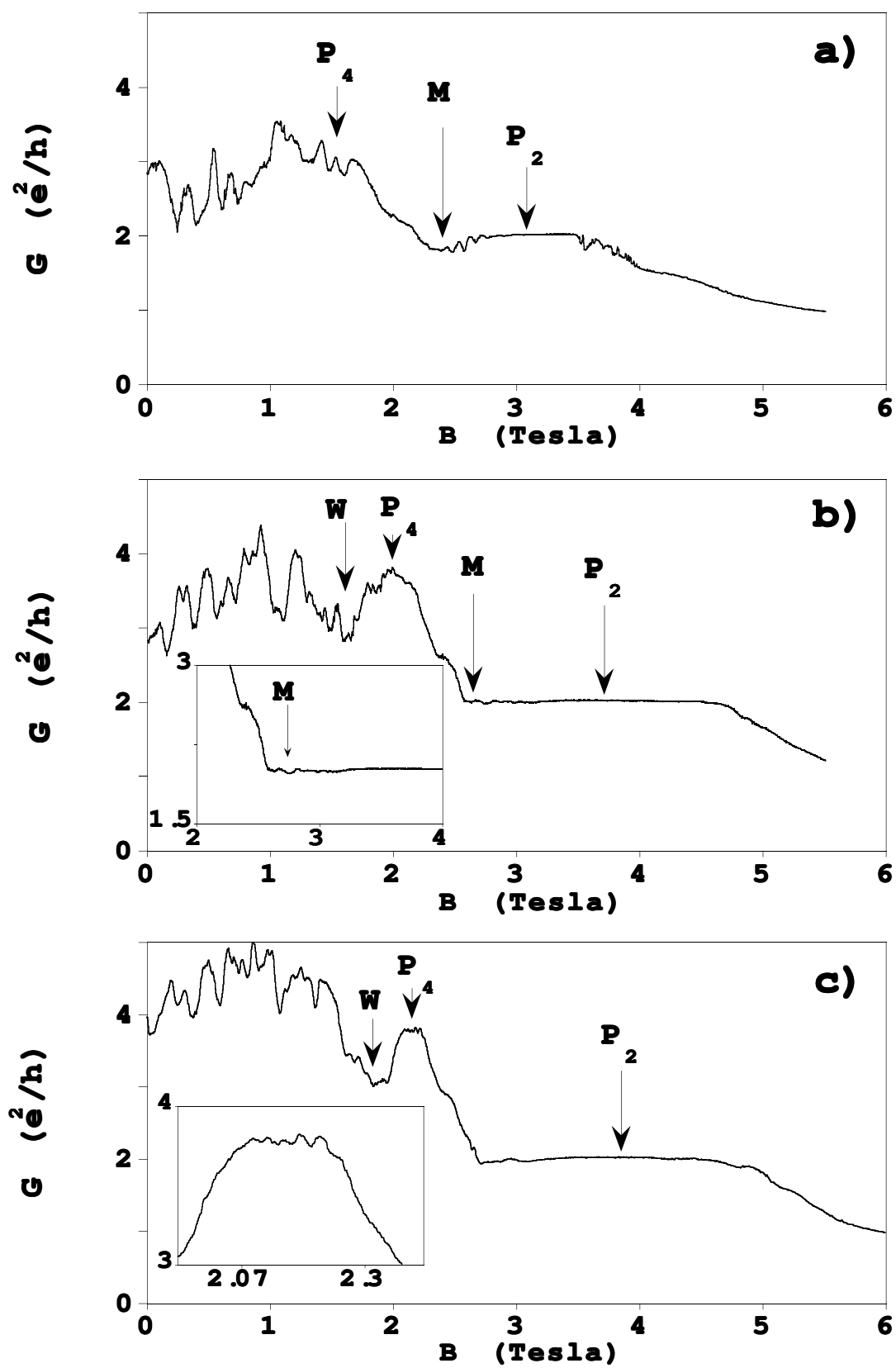
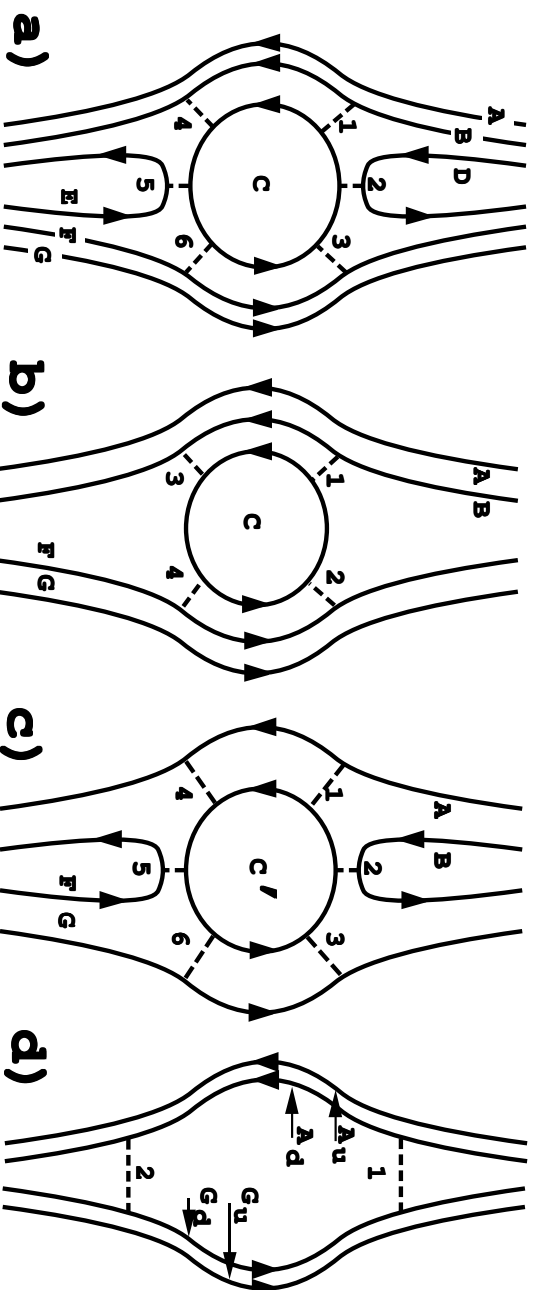


**Figure 3**



**Low Field**  $\longrightarrow$  **High Field**





Figure 4

